A Novel Passive Shoulder Exoskeleton Using Link Chains and Magnetic Spring Joints

Hyun-Ho Lee, Kyung-Taek Yoon, *Graduate Student Member, IEEE*, Hyun-Ho Lim, Won-Kyu Lee, Jae-Hwan Jung, Seung-Beom Kim, and Young-Man Choi

***Abstract*— Work-related musculoskeletal disorders represent a major occupational disability issue, and 53.4% of these disorders occur in the back or shoulders. Various types of passive shoulder exoskeletons have been introduced to support the weight of the upper arm and work tools during overhead work, thereby preventing injuries and improving the work environment. The general passive shoulder exoskeleton is constructed with rigid links and joints to implement shoulder rotation, but there exists a challenge to align with the flexible joint movements of the human shoulder. Also, a force-generating part using mechanical springs require additional mechanical components to generate torque similar to the shoulder joint, resulting in increased overall volume and inertia to the upper arm. In this study, we propose a new type of passive shoulder exoskeleton that uses magnetic spring joint and link chain. The redundant degrees of freedom in the link chains enables to follow the shoulder joint movement in the horizontal direction, and the magnetic spring joint generates torque without additional parts in a compact form. Conventional exoskeletons experience a loss in the assisting torque when the center of shoulder rotation changed during arm elevation. Our exoskeleton minimizes the torque loss by customizing the installation height and initial angle of the magnetic spring joint. The performances of the proposed exoskeleton were verified by an electromyographic evaluation of shoulder-related muscles in overhead work and box lifting task.**

***Index Terms*— Exoskeleton, magnetic spring, link chains, scapulohumeral rhythm, electromyography, gravity compensation.**

I. Introduction

INDUSTRIAL exoskeletons have been developed and used to assist industrial workers in modern work environments and prevent injuries. In particular, 53.4% of work-related musculoskeletal disorders (WMSDs) cause problems in the back and shoulder muscles of industrial workers performing repetitive tasks at overhead heights (e.g. [1], [2]). To alleviate shoulder-related problems, industrial exoskeletons, such as AIRFRAME (Levitate Technologies, USA) [3], ShoulderX (SuitX, USA) [4], H-VEX (Hyundai, Republic of Korea) [5] MATE (Comau, Italy) [6], and PAEXO (Ottobock, Germany) [7] have been developed. In consideration of the industrial environments, passive type of exoskeletons, which uses the elastic force of a mechanical spring without a power source, is mainly adopted (e.g. [8], [9]). The satisfactory performance of these exoskeletons has been confirmed by reduced muscle activity of the shoulder-related muscles before and after wearing them when performing overhead work, showing that they are helpful in improving the user's working ability and preventing shoulder diseases (e.g. [10], [11]).

Conventional passive shoulder exoskeletons incorporate a limited set of links and joints to align shoulder movement while minimizing weight and volume. They generally feature a rotary joint located above the shoulder, enabling cross-body adduction/abduction. Additionally, there is a joint on the side of the shoulder that facilitates two upward rotations, namely flexion/extension and abduction/adduction, of the upper arm. (e.g. [12], [13], [14]). On the other hand, the human shoulder joint consists of the sternoclavicular (SC) joint, scapulothoracic (ST) joint, acromioclavicular (AC) joint, and glenohumeral (GH) joint. The complex movement of these four joints results in the movement of the center of GH joint, which shifts vertically and horizontally when the upper arm upward rotation (e.g. [15], [16]). Such a change in the center of rotation may cause collision with the rotary joint of an exoskeleton fixed above the shoulder. Even if the joint is positioned higher than the shoulder, there is a possibility of collision with the head [17]. Additionally, the fixed joint located above the shoulder makes it challenging to align with horizontal shoulder joint movement and to fit with wearers' diverse body size (e.g. [14], [17]). There has been a study that considered adding offsets to the initial positions of the fixed rotation joints located above the shoulder to account for shoulder collisions [18]. There have been shoulder exoskeletons that place the rotation joints on the back, rather than above the shoulder, to prevent the possibility of collisions (e.g. [19], [20]).

Most passive shoulder exoskeletons use the elastic restoring force of a mechanical spring as a force generating part. The force generating part is coupled with a rotary joint located on the side of the shoulder to generate torque corresponding

Manuscript received 28 June 2023; revised 19 October 2023, 2 January 2024, and 7 January 2024; accepted 22 January 2024. Date of publication 29 January 2024; date of current version 8 February 2024. This work was supported by the National Research Foundation of Korea grant funded by the Korean Government under Grant 2019R1C1C1006067. *(Corresponding author: Young-Man Choi.)*

This work involved human subjects or animals in its research. Approval of all ethical and experimental procedures and protocols was granted by the IRB Ethics Committee of Ajou University under Application No. 2021-HB-EX-001.

The authors are with the Department of Mechanical Engineering, Ajou University, Suwon 16499, South Korea (e-mail: lho3692@ajou.ac.kr; ymanchoi@ajou.ac.kr).

Digital Object Identifier 10.1109/TNSRE.2024.3359658

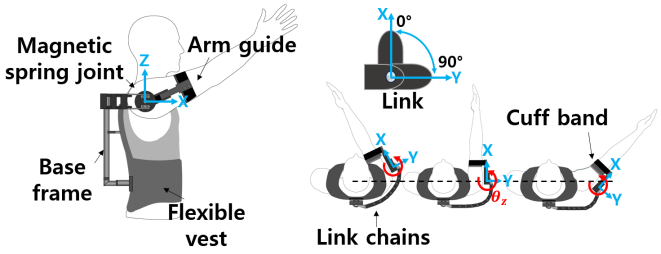

Fig. 1. Proposed shoulder exoskeleton using magnetic spring joints and link chains.

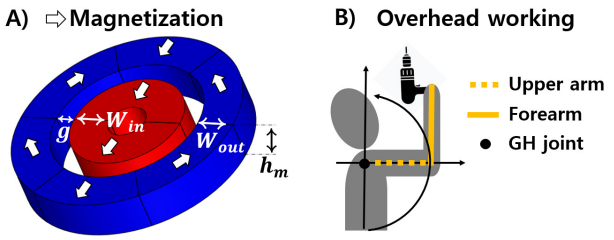

Fig. 2. Design of the magnetic spring joint and target working motion. A) Layout and design parameters of inner and outer magnets (Two segments in the inner magnet and six segments in the outer magnet). B) Posture of the upper arm and forearm at overhead working.

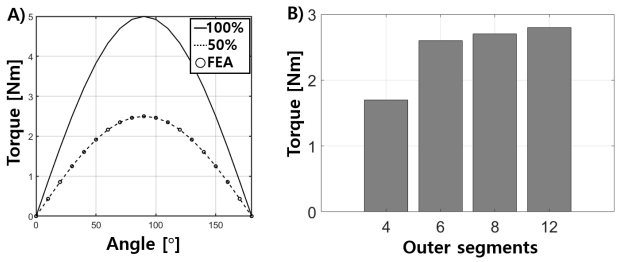

Fig. 3. Torque profiles and maximum torque analysis. A) Overhead working torque profile (solid line), 50% profile (dotted line) and Torque profile of the designed magnetic spring joint (FEA result) (circle). B) Torque vs. the number of segments of the outer magnets.

to the upper arm rotation angle and is fixed together with the upper arm to provide assisting torque (e.g. [12], [13], [14], [18], [21], [22]). However, such force generating part with this structure require transmission mechanisms like cams, pulleys and wires to connect the springs and rotary joints, as well as space for accommodating the tension springs. This increases the volume of the force generating part, which is fixed with the upper arm, potentially compromising comfort during prolonged wear and increasing the risk of collisions with the surrounding environment [23]. So far, there is very little research to address this issue. The PAEXO, a type of passive exoskeleton, locates the force generating part on the back [24].

In this study, we propose a passive shoulder exoskeleton with a compact structure using link chains and magnetic spring joints. We eliminate a rotary joint for horizontal rotation and implement and replace it as link chains which have multiple short links and rotary joints. For a compact force-generating part, we adopt a magnetic spring [25], [26] and integrated it with a rotary joint. To our knowledge, there is no study to use a magnetic spring as a force generator or gravity compensator in passive exoskeletons. A torque transmission model is analyzed considering scapulohumeral rhythm and the kinematics of our exoskeleton. The design parameters were determined through the use of the model, and the exoskeleton was tested by human experiments.

II. Design of Shoulder Exoskeleton

The proposed shoulder exoskeleton is shown in Fig. 1, in which a height-adjustable base frame parallel to the spine is attached to a wearable fabric vest. Link chains are placed along the back from the base frame to a magnetic spring joint located to the side of the shoulder, serving as an upward rotation joint. The magnetic spring joint is connected to an arm guide transmitting the assisting torque to the shoulder joint. The end of the arm guide is attached to the center of the upper arm by a fabric cuff band. Kinematically, the proposed exoskeleton is designed with a total of five degrees of freedom (DOF): two translational and one rotational DOF from link chains, one rotational DOF from the magnetic spring joint, and one translational DOF from the arm guide. Human shoulder joint has also five degrees of freedom due to the 2-axis rotation of the GH joint and the 3-axis translation of the center of the GH joint [16]. The magnetic spring joint corresponds to the degree of freedom to rotate the upper arm up and down. The link chains have one rotational DOF and two translational DOF which enable to track the horizontal shoulder rotation and horizontal shoulder displacement. Additionally, the 90° bending radius of each link allows rotation in only one direction and restricts the upper arm from rotating backward behind the body during cross-body abduction [27]. The prismatic joint used in the arm guide can follow the movement of the upper arm when the shoulder is raised.

The magnetic spring joint, as shown in Fig. 2A, consists of inner magnet and outer magnet. Relative rotation of the inner magnet to the outer magnet generates torque according to the rotation angle as depicted in Fig. 3A. Because the magnetic spring joint is absent from additional mechanical components to transmit torque, the proposed exoskeleton can be designed for compactness by minimizing the volume of the force-generating component. This reduction not only decreases the chances of collisions with the work environment but also enhances overall wearability.

A. Design of the Magnetic Spring Joint

The magnetic spring joint transmits torque without contact through magnetic forces between two magnetic rotors in form of a magnetic bearing or a rotational spring [28]. The proposed magnetic spring joint uses a permanent magnet coupling (PMC) structure (e.g. [29], [30]) in Fig. 2A. In the proposed exoskeleton design, the inner magnet rotates along with the upper arm while the outer magnet is fixed to the end of the link chains. Two magnetic flux loops are generated by the rotating magnetization of the outer magnet, which is realized by fan-shaped segmented magnets practically. The inner magnet is designed to have a single magnetization direction to rotate along the magnetic field of the outer magnet.

First and foremost, the assisting torque profile must be determined to design the magnetic spring. Fig. 2B shows an overhead task with the upper arm raised 90° about the GH joint. If we assume that the distance between the hand and shoulder is maintained during arm elevation, the shoulder torque is calculated to be sinusoidal as shown in Fig. 3A. At this time, the torque is calculated from the anthropometric data for upper arm weight [31] and a tool weight of 1.2 kg. The maximum assisting torque of 2.5 Nm, which is 50% of the maximum shoulder torque, is selected to prevent possible injury due to the magnetic spring forcibly rotating the upper arm.

Since the number of segments affect the magnetic field, the maximum torque of the magnetic spring was investigated for the number of outer magnet segments using finite element analysis (FEA). FEA used the Maxwell software (Ansys Inc.), and 5000 tetrahedral meshes for each inner magnet and outer magnet were used. Also, NdFeB45 grade with a Br value of 1.35 T were used for magnets. As shown in Fig. 3B, the torque increases with the number of segments but the difference in torque was relatively small with six segments or more; therefore, six segments were selected for the outer magnet considering assembly issues and fabrication tolerances.

The design parameters to determine torque profile of the magnetic spring joint include the radius of the shaft (r_{ms}), the width of the inner magnet (W_{in}), the air gap between the inner magnet and the outer magnet (g), the width of the outer magnet (W_{out}) and the height of the magnets (h_m). The total radius of the magnetic spring joint is as

$$r_{ms} = r_{shaft} + W_{in} + g + W_{out} \tag{1}$$

The radius of the magnetic spring joint should be made smaller than the shoulder size of around 80 mm (average radius of the humerus (25 mm), skin thickness (15 mm)) to avoid interference with working environment (e.g. [32], [33]). So, the radius of the magnetic spring joint is selected to be 30 mm (the total diameter of the magnetic spring joint including the cage is 78 mm). The radius of the shaft and the gap were set to 5 mm and 1 mm, respectively, considering the fabrication and assembly. Because the radius of the magnetic spring joint is fixed, the torque profile of the magnetic spring joint depends on the width of the inner magnet and the height of the magnet. It was assumed that the heights of the inner and outer magnets were the same. Fig. 4A and B shows the torque per unit weight calculated by 3D FEA when the W_{in} and h_m change by 1 mm. The minimum size of the W_{in} and h_m are 5 mm, and analysis was performed for the W_{in} up to 19 mm and h_m up to 17 mm. As a result of the analysis, the height of the magnet increases, the torque per unit weight also increases monotonically, while the torque per unit weight reaches its maximum value at a width of 14 mm of the inner magnet regardless of h_m. With W_{in} fixed as 14 mm, the torque and weight for changes in h_m were analyzed as shown in Fig. 4C. The height of the magnet with the lowest weight while satisfying the target torque of 2.5 Nm or more was found as 13 mm. Finally, the W_{in} of the magnetic spring joint was selected as 14 mm and the h_m as 13 mm.

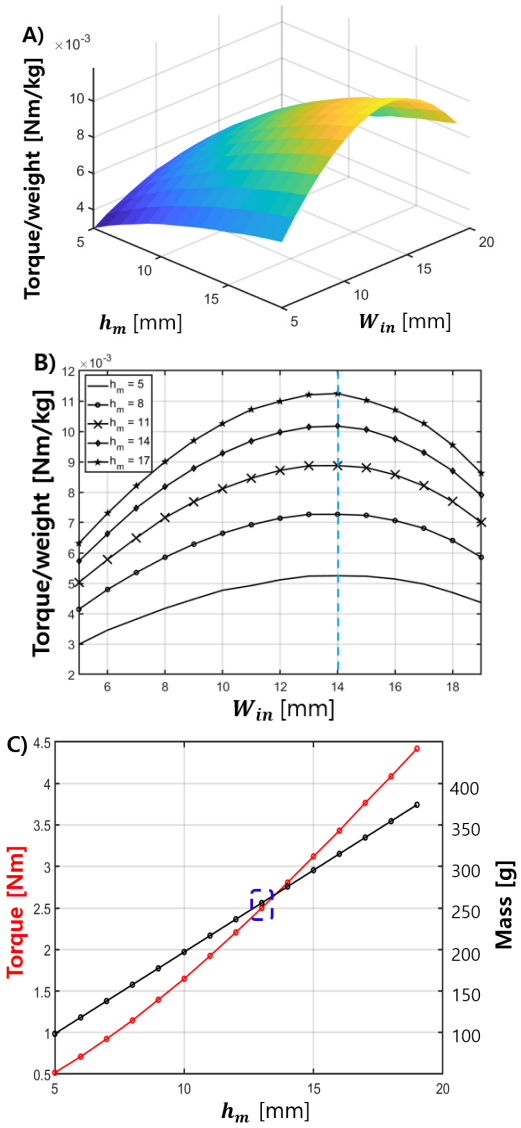

Fig. 4. FEA result of the magnetic spring joint. A) 3D plot of the torque/weight for the W_{in} and h_m. B) 2D plot of the torque/weight for the W_{in} and h_m. C) Torque and mass results for the h_m.

TABLE I
DIMENSIONS OF THE MAGNETIC SPRING JOINT

Parameters	Dimensions
W_{in} (mm)	14
W_{out} (mm)	10
h_m (mm)	13
g (mm)	1
Weight (g)	255

Table I lists the dimensions of the designed magnetic spring joint. The calculated torque profile from the FEA is depicted in Fig. 3A as circular markers precisely matching the target profile.

Fig. 5 shows the 3D drawings of the magnetic spring joint. The outer magnet is contained in a plastic cage connecting to the end of the link chain, and the inner magnet is fixed on a shaft to rotate with the upper arm. Ball bearings are integrated to ensure smooth rotation.

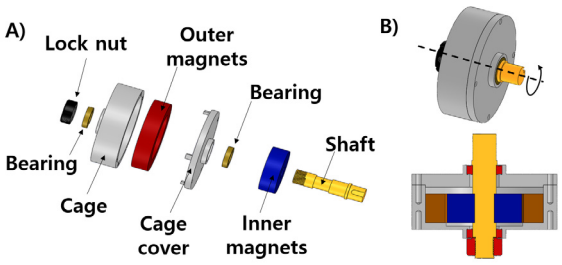

Fig. 5. Schematic of a magnetic spring joint. A) Exploded view. B) Axial cross-section view.

B. Assisting Torque Mismatch

The upward rotation joint position of an exoskeleton and the center of rotation (CoR) of the GH joint should be considered to confirm the assisting torque transmitted to the shoulder joint. The link chain can follow the GH joint CoR translating in the X-Y planes. However, in the transverse plane, there occurs a mismatch between the positions of two joints due to the shoulder elevation. In a previous study, the location of the GH joint in the transverse plane, Z_{CoR}, was modeled as a function of the arm angle only [16]. As shown in Fig. 6A, the Z_{CoR} elevates when the arm angle θ_{arm} increases. If the magnetic spring joint CoR or an effective force-generating part CoR of a conventional exoskeleton is located at the height h_0 from the GH joint CoR when $\theta_{arm} = 0°$, the height difference Δh between Z_{CoR} and h_0 is determined as

$$\Delta h = Z_{CoR}(\theta_{arm}) - h_0 \tag{2}$$

From the fixed distance l_u between the GH joint CoR and the arm cuff at the point of action on the upper arm, the position of the cuff in the X-Z plane, x_u and z_u, is calculated as

$$x_u = l_u \sin(\theta_{arm}) \tag{3}$$

$$z_u = Z_{CoR}(\theta_{arm}) - l_u \cos(\theta_{arm}) \tag{4}$$

To follow the position change of the arm cuff, the length l_g of the arm guide is determined as

$$l_g = \sqrt{(x_u)^2 + (z_u - h_0)^2} \tag{5}$$

On the other side, the change in Z_{coR} causes an angular difference θ_{dev} between θ_{arm} and the rotation angle of the exoskeleton θ_{exo} as

$$\theta_{dev} = \theta_{exo} - \theta_{arm} \tag{6}$$

where

$$\theta_{exo} = \left[\pi - \tan^{-1}\left(\frac{x_u}{z_u - h_0}\right)\right] \tag{7}$$

The actual assisting torque τ_{assist} transmitted to the shoulder is reduced by the effect of θ_{dev} as

$$\tau_{assist} = f_{exo}\cos(\theta_{dev}) \times l_u \tag{8}$$

$$\tau_{assist} = \tau_{exo}\cos(\theta_{dev}) \times \frac{l_u}{l_g} \tag{9}$$

Depending on the θ_{arm} and h_0, the assisting torque profile deviates from the ideal sine profile to support the shoulder joint. However, the torque deviation can be minimized by adjusting the h_0 and the initial angle (θ_{ms_0}) of the magnetic spring joint. Because θ_{ms_0} of the magnetic spring joint is adjustable, the assisting torque by the exoskeleton τ_{exo} is defined as

$$\tau_{exo} = \tau_{\max}\sin(\theta_{exo} + \theta_{ms\_0}) \tag{10}$$

where τ_{max} denotes the maximum torque in the sine torque profile, as shown in Fig. 3A. Finally, by substituting Eq. (6), Eq. (7) and Eq. (10) to Eq. (9), the assisting torque τ_{assist} of the proposed device can be represented as

$$\begin{aligned}\tau_{assist} &= \tau_{\max}\sin\left[\tan^{-1}\left(\frac{l_u\sin(\theta_{arm})}{z_{CoR}(\theta_{arm}) - l_u\cos(\theta_{arm}) - h_0}\right) - \theta_{ms\_0}\right] \\ &\quad \times \cos\left[\theta_{arm} + \tan^{-1}\left(\frac{l_u\sin(\theta_{arm})}{z_{CoR}(\theta_{arm}) - l_u\cos(\theta_{arm}) - h_0}\right)\right] \\ &\quad \times \frac{l_u}{\sqrt{(x_u)^2 + (z_u - h_0)^2}} \\ &= f(h_0, \theta_{ms\_0})\end{aligned} \tag{11}$$

If the upward rotation joint, identified as the magnetic spring joint in this context, is positioned at shoulder height with the arm angle set to 0°, the maximum torque occurs at approximately 65°, deviating from the initially intended 90°, as illustrated by the solid line in Fig. 6B. This is due the mismatch between the exoskeleton joint and shoulder joint. However, in our exoskeleton, we can change the torque profile by adjusting h_0 and θ_{ms_0} as described in Fig. 6B and C. HLX is a notation corresponding the height of the magnetic spring joint, h_0. Because the height in mm may not be applicable to every individual, HLX is defined as the height of shoulder joint at the arm angle θ_{arm} = X, which elevates in scapulohumeral rhythm. Higher level of HLX leads the shift of the maximum torque angle to a larger angle. Next, the initial angle of the magnetic spring joint θ_{ms_0} allows for adjustments in the maximum torque angle and corresponding magnitude in the range of 0° to 20°. When adjusted by more than 20°, it starts affecting the range of flexion for overhead tasks (20° to 100°) [27].

In this study, we choose the maximum torque angle located at 100°, which human shoulder generates maximum torque [14]. This is due to the change of the shoulder CoR with natural shoulder elevation. Simply, the magnetic spring height of HL150 (corresponding to the shoulder joint height at arm angle of 150°) can obtain the maximum torque angle of 100°. However, as the magnetic spring height is set too high, the magnetic spring joint protrudes above the shoulder. Ultimately, HL100 and an initial angle of 10° were selected to minimize the installation height of the magnetic spring joint ensuring that the maximum torque occur at the arm angle of 100° without a significant loss in torque below 100°.

III. Evaluation of Shoulder Exoskeleton

A. Prototype Fabrication

Fig. 7 shows the fabricated magnetic spring joint and entire shoulder exoskeleton. The magnetic spring joint was fabricated using an outer magnet consisting of six segments and an

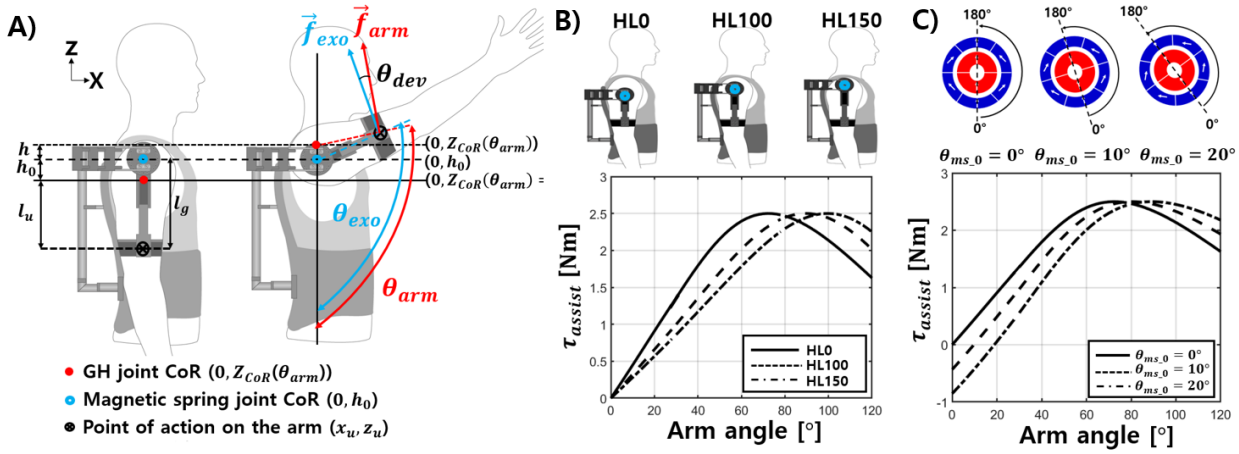

Fig. 6. Assisting torque mismatch model. A) Schematic of the exoskeleton and CoR change according to the arm elevation. B) Assisting torque profiles for the height of the magnetic spring joints. HLX corresponds the shoulder height when the arm angle is X°. C) Assisting torque profiles for the initial angle of the magnetic spring.

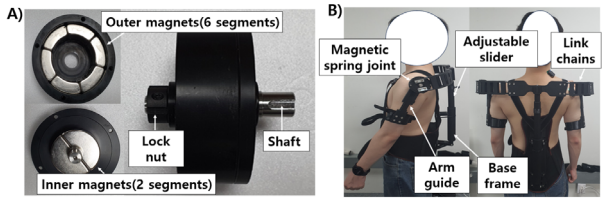

Fig. 7. Fabricated shoulder exoskeleton. A) The magnetic spring joint. B) User-worn exoskeleton.

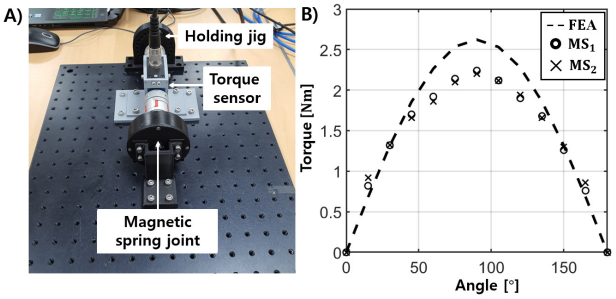

Fig. 8. Evaluation of the magnetic spring joints. A) Experimental setup to measure torque of the magnetic spring joints. B) Measured torques and calculated torque from the FEA.

inner magnet consisting of two segments. For the link chains, commercial link chains (MHPKS204-38-20-A, Misumi) was used. The base frame and arm guide were fabricated by a 3D printer (Pro2 dual 3D printer, Raise3D) using polylactic acid. Based on the results of the torque model, the arm guide was fabricated to have 65 mm range (Eq. (5)). The total weight of the exoskeleton is 1.9 kg. The inertial load to the upper arm weighed only 400 g including the shaft, the inner magnet, an arm guide, and a cuff.

B. Evaluation of the Magnetic Spring

The fabricated magnetic spring was evaluated using a torque sensor (4502A, Kistler). The magnetic spring can be fixed at every 15° using a holding jig, as shown in Fig. 8A. The torques of the two magnetic springs (MS_1 and MS_2) for both sides of the shoulder, were measured over the shoulder range (0°–180°) when performing overhead work, as shown in Fig. 8B. The mean torque error is 12.0% for MS_1 and 10.4% for MS_2 when compared with the calculated torque from the FEA.

C. Range of Motion

The assessment of exoskeletal range of motion (ROM) can be performed using methods based on Denavit-Hartenberg (D-H) parameters for forward or inverse kinematics calculations. However, these approaches have limitations because each wearer has a different body size, device wearing position, and GH joint movement profile. In this study, an experimental approach is chosen to enhance the objectivity of shoulder ROM assessment before and after wearing the device [34]. To evaluate the ROM of the proposed exoskeleton, a visual examination of an adult male (age: 27 years, height: 168 cm, weight: 81 kg, upper arm: 20 cm, forearm: 37 cm) was performed. The length of the upper arm was measured from the greater tubercle of the humerus, where the GH joint is located, to the olecranon using a ruler. Similarly, for the forearm, measurements were taken from the olecranon to the tip of the middle finger. Additionally, the number of link chains was adjusted to match the subject's body length before the experiment. Fig. 9 shows the experimental setup using eight optical cameras (Primex13, OptiTrack) with 1.3M pixels and a frame rate of 240. Additionally, 27 optical markers for measuring positions were attached to the upper limbs. Measurements were performed for three shoulder tasks: ABD/ADD in the coronal plane, FL/EX in the sagittal plane, and C-ADD/C-ABD in the transverse plane. ROMs were measured by the position of the marker at the fingertip (end point) for two conditions: without assistance (WO) and with assistance (WA) from the exoskeleton. During the measurement, the maximum extension of the elbow and wrist was maintained.

D. Muscle Evaluation

Muscle activity evaluation was conducted on five healthy adult males with various body sizes, as shown in TABLE III,

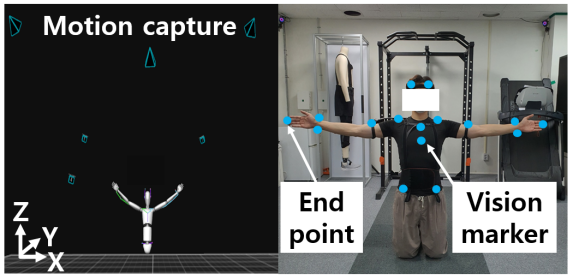

Fig. 9. Experimental setup for shoulder range of motion using motion capture optical cameras and vision markers.

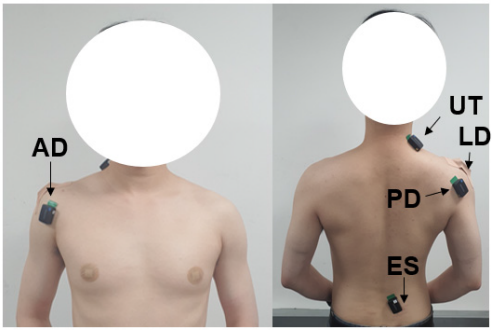

Fig. 10. EMG electrodes applied to 3 deltoid (anterior, lateral, posterior) muscle, 1 trapezius (upper) muscle, and 1 erector spinae muscle.

to demonstrate the effects of the device. Fig. 10 depicts the attachment locations of surface electromyography (sEMG) sensors (Trigno Wireless Biofeedback System, Delsys) used for muscle activity evaluation. The sensors were located on the anterior deltoid (AD), lateral deltoid (LD), and posterior deltoid (PD) muscles connected to the GH joint and the upper trapezius (UT) muscle, which is involved in the GH joint's rotational center translation. Additionally, the erector spinae (ES) muscle, responsible for bearing the weight of the device when worn, was assessed (e.g. [14], [18], [22], [24]). The sEMG sensors were collected at a sampling rate of 2000 Hz. Prior to the evaluation, Maximum Voluntary Isometric Contraction (MVIC) for each muscle were measured with 3 repeated measurements in an isolated position to compare muscle activity before and after exoskeleton. These measurements were conducted in accordance with the SENIAM guidelines [35].

Fig. 11A is a typical overhead drilling performed in automotive and manufacturing processes. A static performance at an arm angle of 100° using a 1.2 kg hand drill is performed in a laboratory environment. At this time, the installation height level of the magnetic spring is manually adjusted and fixed according to the center of rotation of the shoulder at the subject's arm posture of 100° according to the parameter learning result of Section II-B. In addition to overhead drilling, industrial workers in construction environments are often required to lift objects. In order to evaluate the performance of the exoskeleton for these lifting tasks, an experiment is conducted on the lifting a box (weight: 5 kg, volume: equal to the width of both shoulders) as shown in Fig. 11B. First, the subjects practice the working motion before wearing the exoskeleton. Then holding the drill and elevation an arm to 100° for

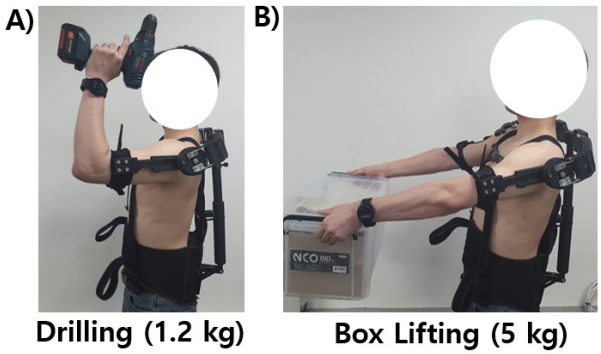

Fig. 11. Two tasks for muscle evaluation at without assistance (WO) and with assistance (WA). A) Overhead drilling task. B) Box lifting task.

3 seconds and hold the position for 7 seconds. This operation is repeated 10 times with a 5-minute break, and is performed WO and WA, respectively. The measured sEMG signals from each muscle were processed by removing the initial offset and passing through a 4th-order Butterworth band-pass filter and a 60 Hz notch filter. The processed signals were then used to calculate the Root Mean Square (RMS) values during a 7-second period of maintaining the posture, followed by obtaining the average. Subsequently, the data was normalized using the pre-experiment measured MVIC. Additionally, for objective evaluation, a statistical test was performed using the t-test function provided by Matlab (MathWorks Inc.). Then, Cohen's d-value was analyzed to determine the effect size due to assisting torque [36].

IV. Experimental Results

Fig. 12A shows the result of the ABD task from an arm angle of 0° to the maximum movable angle on the Y-Z plane. The ADD task was then performed from the end of the ABD position to the maximum movable angle. Fig. 12B shows the FL/EX tasks in the X-Z plane at the same starting point and procedure as that of ABD/ADD. In the case of the C-ADD/C-ABD tasks shown in Fig. 12C, the point of the arm angle at 90° in flexion was the starting point in the X-Y plane. The C-ABD task was performed to rotate the arm outward as much as possible. Then, the C-ADD task was performed to rotate the arm inward again. TABLE II presents the ROMs for both the conditions (WO and WA) for the three exercises. The proposed exoskeleton did not hinder the shoulder's ROM in ABD/ADD and FL/EX. Only in the case of C-ADD/C-ABD, the ROM was limited after 90° rotation.

Fig. 13 and Table IV present the experimental results for WO and WA for drilling and box lifting. In the case of drilling, as shown in Fig. 13A, there was a decrease in muscle activity when WA, with a reduction of 30.3% in the AD, 15.9% in the LD, and 14.4% in the PD. On the other hand, the UT showed an increase of 2.5% in muscle activity, and the ES exhibited an 18.0% increase in muscle activity. Statistical analysis revealed significant effects of the device on the AD ($p = 0.006$) and the ES ($p = 0.026$) for drilling. In terms of effect size (d- values), the AD ($d = 0.427$) showed a moderate effect ($d = 0.5$), while the ES ($d = 0.383$) exhibited an effect size between small ($d = 0.2$) and moderate ($d = 0.5$). Fig. 13B shows the results

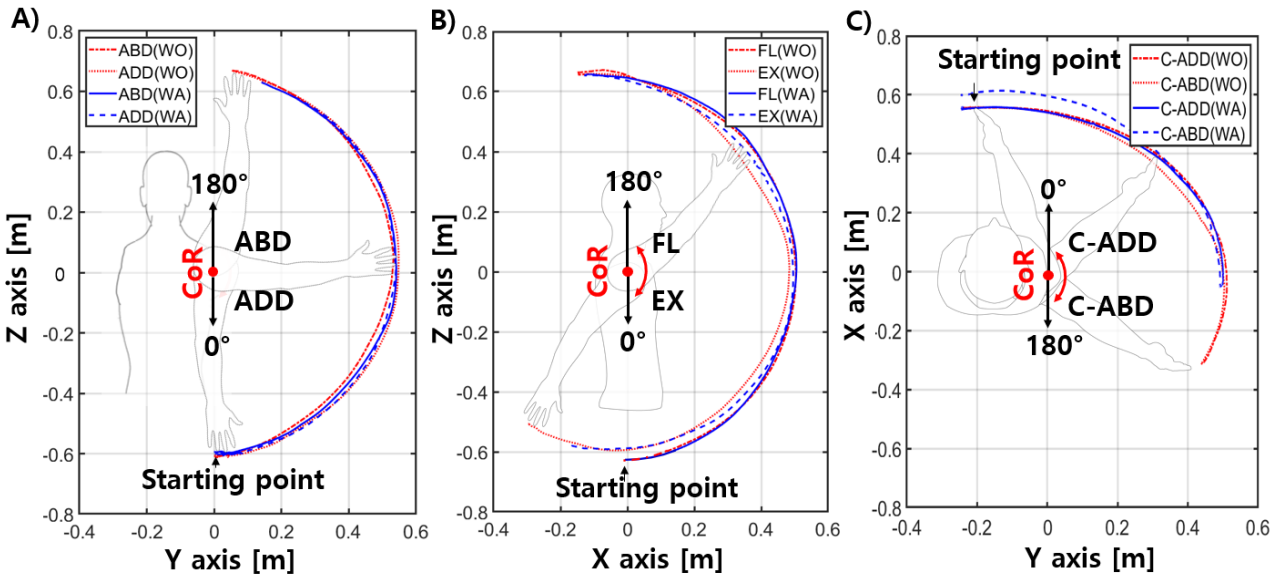

Fig. 12. Experimental results of shoulder ROM for without assistance (WO) and with assistance (WA). A) Abduction (ABD)/Adduction (ADD) in the Y-Z plane. B) Flexion (FL)/Extension (EX) in the X-Z plane. C) Cross body Adduction (C-ADD)/Abduction (C-ABD) in the X-Y plane.

TABLE II
EXPERIMENTAL RESULTS OF THE SHOULDER ROM FOR WITHOUT ASSISTANCE(WO) AND WITH ASSISTANCE(WA)

Variables	Shoulder Range of Motion (°)					
	ABD	ADD	FL	EX	C-ADD	C-ABD
WO	0 ~ 176	176 ~ 0	0 ~ 190	190 ~ -29	-10 ~ 134	134 ~ -10
WA	0 ~ 165	165 ~ 0	0 ~ 189	189 ~ -17	-10 ~ 97	97 ~ -10

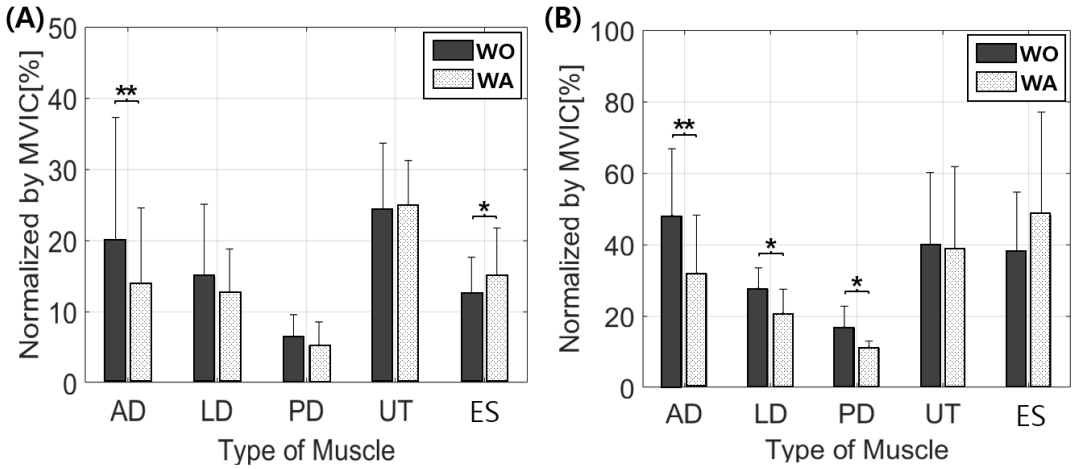

Fig. 13. Overhead working for muscle activities of AD, LD, PD, UT, and ES ($^*p < 0.05$, $^{**}p < 0.01$). EMG amplitude normalized by MVIC for A) drilling and B) Box lifting.

of muscle activity during box lifting. In this case, the AD decreased by 33.7%, the LD decreased by 25.2%, and the PD decreased by 33.3%. Furthermore, the UT showed a slight decrease of 2.8%, while the ES increased by 26.7%. The statistical results indicated significant differences in all three deltoid muscles: AD ($p = 0.004$), LD ($p = 0.016$), and PD ($p = 0.016$). The d-value also shows that the effect size of the AD ($d = 0.848$), LD ($d = 0.984$), and PD ($d = 1.099$) is large ($d = 0.8$) or higher. For the ES, the results were very close to statistical significance ($p = 0.05$) with a $p = 0.065$. The effect size (d-value) was 0.443, indicating a moderate-sized effect. Additionally, because the magnetic spring joint only provides upper arm upward torque, human body evaluation was performed on upper arm downward motion during drilling and box lifting tasks. Fig. 14 illustrates the differences in muscle activity (ΔEMG) for WO and WA during the downward of the arm after 7 seconds in both drilling and box lifting tasks for each participant. In this case, we focused on the AD muscle, which showed statistically significant results (p <0.01) for both drilling and box lifting tasks. Contrary to the expected

TABLE III
PARTICIPANTS OF THE MUSCLE ACTIVITY EVALUATION

Subject	Age [years]	Weight [kg]	Height [cm]	Upper arm [cm]	Forearm [cm]
1	24	78	173	27	44
2	25	59	171	25	44
3	27	72	174	26	45
4	29	63	170	25	43
5	30	78	186	28	47

TABLE IV
OVERHEAD DRILLING AND BOX LIFTING TASK PERFORMANCES FOR WITHOUT ASSISTANCE(WO) AND WITH ASSISTANCE(WA)

Drilling	Type of Muscle				
	AD	LD	PD	UT	ES
WO (%)	19.77 (17.42)	14.96 (10.11)	6.11 (10.73)	24.26 (9.42)	12.50 (5.15)
WA (%)	13.78 (10.73)	12.57 (6.27)	5.23 (6.27)	24.87 (6.40)	14.76 (6.92)
ΔEMG (%)	-30.3 ($t(4)$=5.162, p=0.006, d=0.427)	-15.9 ($t(4)$=-0.072, p=0.946, d=0.296)	-14.4 ($t(4)$=1.387, p=0.237, d=0.275)	+2.5 ($t(4)$=-0.776, p=0.480, d=0.080)	+18.0 ($t(4)$=-3.437, p=0.026, d=0.383)
Box lifting	AD	LD	PD	UT	ES
WO (%)	47.99 (18.87)	27.56 (5.88)	16.73 (5.93)	39.79 (20.41)	37.99 (16.75)
WA (%)	31.80 (16.38)	20.61 (6.87)	11.17 (1.75)	38.69 (23.02)	48.15 (28.88)
ΔEMG (%)	-33.7 ($t(4)$=5.657, p=0.004, d=0.848)	-25.2 ($t(4)$=3.966, p=0.016, d=0.984)	-33.3 ($t(4)$=4.006, p=0.016, d=1.099)	-2.8 ($t(4)$=1.233, p=0.284, d=0.053)	+26.7 ($t(4)$=-2.514, p=0.065, d=0.443)

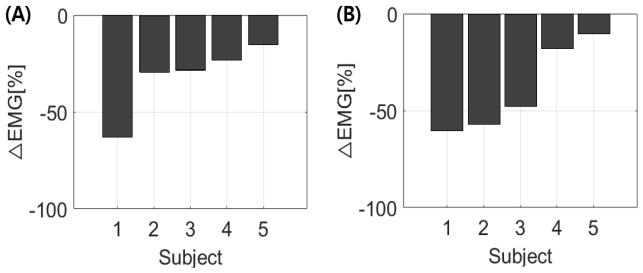

Fig. 14. Results of ΔEMG (AD muscle) during upper arm lowering for 5 subjects. A) Drilling and B) Box lifting.

increase in muscle activity due to the resistive torque of the magnetic spring joint, all subjects exhibited a decrease in muscle activity (Average 31.4%). The statistical results also confirmed significant results at $p = 0.017$.

Fig. 14B shows the results for arm downward after box lifting. Similar to drilling task, all five subjects exhibited a decrease in muscle activity, with an average reduction of 38.3%. Statistical analysis ($p = 0.021$) also confirmed a significant correlation. The effect size (d-value) for downward arm after drilling was small ($d = 0.278$), while for downward arm after box lifting, it was of moderate size ($d = 0.498$).

V. DISCUSSION

For the fabricated magnetic springs, they have slightly smaller torque than expected by the FEA. The torque error of the magnetic spring can be largely attributed to two factors: First is the variation of the magnetization. The magnet used in the magnetic spring is NdFeB45 grade magnet with a remanence B_r is between 1.32 and 1.38 T according to the manufacturer's specifications. This variation may cause an error of 4.4% compared to 1.35 T used in the simulation. In real, there might be more variation in the magnetization. Second, the magnet spring has assembly tolerances and dimensional tolerances. The gap between magnets occurs inevitably when they were manufactured through forced bonding. It is challenging for the FEA model to incorporate such assembly-related tolerances, leading to the possibility of those torque errors.

In Section III-C, we demonstrated unrestricted range of motion during flexion and abduction in the direction of upper arm upward rotation. The proposed exoskeleton restricts horizontal shoulder rotation by a limited bending radius of 90° in each link chain. As shown in Fig. 10C, the cross-body abduction is successfully limited to 97° ensuring that the link chains operate without folding backward and forms a compact shape around the posterior part of the back.

Section III-D shows the performance for overhead drilling and box lifting task using the proposed exoskeleton. Both tasks in WA showed a significant reduction in muscle activity of more than 30% for AD muscle. AD muscle has a high risk of injury during these kinds of tasks acting as a primary agonist muscle for arm elevation. Our result agrees with those of the commercial exoskeletons (e.g. [14], [18], [22], [24]).

In the case of drilling task, all deltoid muscles showed a decrease in muscle activity when WA However, statistical analysis ($p = 0.006$) revealed that the AD, responsible for contracting the upper arm forward as it elevates, played a significant role in this movement. The effect sizes (d-values) for the LD ($d = 0.296$) and PD ($d = 0.275$) showed small effect sizes, while the AD ($d = 0.427$) exhibited an effect size close to moderate ($d = 0.5$). These results support the notion that the AD plays a significant role during drilling task, with a moderate effect size, compared to the smaller effects observed in the LD and PD. On the other hand, the UT showed a slight increase, averaging 2.5%. However, the results were not statistically significant ($p = 0.480$) and exhibited a very small effect size ($d = 0.080$). These findings suggest that the device had little impact on the UT muscle. On the other hand, during drilling task, the muscle activation of the ES increased by 18.0% in WA. The statistical analysis showed a significant impact ($p = 0.026$) due to the device's weight, but with an effect size of $d = 0.383$, it confirmed that the strain on the lower back was at a relatively small level. In the case of box lifting task, unlike drilling task, statistically significant results ($p < 0.05$) were observed in all deltoid muscles showing a large effect size of $d = 0.8$ or greater. It requires anterior and lateral rotation of the upper arm to grasp a large box, which has a significant impact on the activation of all-deltoid muscles. For the UT, there was a slight decrease of 2.8% in muscle activity, but both the statistical results ($p = 0.284$) and the very small effect size ($d = 0.053$) indicate that there is no significant correlation with the assistance of the exoskeleton. In the case of the ES, the muscle activity increased by 26.7% in WA. Although it did not meet statistical significance ($p = 0.065$), it can be inferred that wearing the device places a certain level of strain on the lower back. An increase in load on the lower back is a common issue with rigid structure shoulder exoskeletons. Using a suit and wires can be a potential solution, but it comes with its own set of problems, such as a reduction in transmitted torque due to wire friction and issues like skin chafing (e.g. [37], [38]). Additionally, the experimental results for the downward rotation of the arm during drilling and box lifting task indicate that the assistance is effective at the lowe arm angles. In the AD during WA, both drilling (ΔEMG = 31.4%) and box lifting (ΔEMG = 38.4%) resulted in a similar decrease to the main tasks, with $p < 0.05$. These results indicate that eccentric contractions occur to maintain dynamic balance the workload, and the device provides auxiliary torque for stable downward rotation.

Passive exoskeletons so far have shown different assisting torque and muscle activity reduction results. In [14], the exoskeleton enabled a reduction in deltoid muscles, 57% for AD and 72% for LD, at an assisting torque of 10 Nm. In [18], providing 9.5 Nm of assisting torque, AD and LD showed a decrease of 32.4% and 45.2%, respectively. Both studies utilized a tool of a weight of approximately 2 kg. Some exoskeletons had much smaller torque level. In [20], providing a similar level of assisting torque (3 Nm) to our study, the muscle activity of AD decreased by 21.5%. In [22], with a 4 Nm assisting torque, AD showed an 18% decrease, while LD showed a 20% decrease. Our shoulder exoskeleton revealed a 30% reduction in AD muscle activation during drilling and lifting tasks at 2.5 Nm of assisting torque. This level of reduction is comparable to that seen in other exoskeletons providing assistance torque of 3 Nm or more, excluding [14]. It demonstrates that, even with small torque, sufficient assistance torque can be achieved by optimizing the height of the force generator to suit the wearer considering shoulder elevation. Furthermore, while a high level of assisting torque offers substantially benefits the shoulder muscles, it concurrently escalates the reaction force on supporting parts, thereby increasing the activity of ES muscle [14], [18]. Consequently, it is recommended to design the passive exoskeleton with the lowest possible torque for adequate assistance, integrating a lightweight structure and a height adjustment function.

VI. Conclusion

In this study, we proposed a passive shoulder exoskeleton using magnetic springs and link chains. The link chains feature a compact structure that conforms to the wearer's body, preventing collisions with the device during shoulder elevation and allowing alignment for flexible shoulder joint movements during horizontal shoulder rotation. The magnetic spring joint reduces the volume of the force generating part and eliminates the transmission part fixed to the upper arm. With the torque model, we pointed out that the conventional exoskeleton with a rotary joint installed at the shoulder height at rest exhibit a maximum torque at much lower arm angle than 90° which may lose torque at the designated task. In order to prevent this loss, it is confirmed that the exoskeleton needs to adjust the height of the rotary joint suitable for user's body size. Considering the mismatch between the exoskeleton and shoulder, the installation height level and initial angle of the magnetic spring joint were selected to minimize the loss of assisting torque.

In both overhead drilling and box lifting tasks, we confirmed a significant reduction in deltoid muscle activity, indicating improved efficiency and reduced strain on the shoulder muscles. Furthermore, during the downward after drilling and box lifting task, there was a reduction more than 30% in muscle activity of the AD muscle. This reduction is attributed to the relieved eccentric contraction by the assistance of the proposed exoskeleton.

References

[1] J. K. Sluiter, K. M. Rest, and M. H. Frings-Dresen, "Criteria document for evaluating the work-relatedness of upper-extremity musculoskeletal disorders," *Scand. J. Work Environ. Health*, vol. 27, pp. 1–102, Jan. 2001.
[2] J. R. Grieve and C. R. Dickerson, "Overhead work: Identification of evidence-based exposure guidelines," *Occupational Ergonom.*, vol. 8, no. 1, pp. 53–66, Sep. 2008.
[3] (Sep. 2023). *Levitate Technologies, Inc*. [Online]. Available: https://www.levitatetech.com/airframe/
[4] (Sep. 2023). *Suitx*. [Online]. Available: https://www.suitx.com/
[5] (Sep. 2023). *Hyundai*. [Online]. Available: https://tech.hyundaimotorgroup.com/kr/convergence/robotics/
[6] (Sep. 2023). *Comau*. [Online]. Available: https://www.comau.com/EN/
[7] (Sep. 2023). *Ottobock*. [Online]. Available: https://www.ottobock.com/en/company/ottobock-industrials/paexo/

[8] A. Voilqué, J. Masood, JC. Fauroux, L. Sabourin, and O. Guezet, "Industrial exoskeleton technology: Classification, structural analysis, and structural complexity indicator," in *Proc. Wearable Robot. Assoc. Conf. (WearRAcon)*, Mar. 2019, pp. 13–20.

[9] A. Moyon, E. Poirson, and J.-F. Petiot, "Experimental study of the physical impact of a passive exoskeleton on manual sanding operations," *Proc. CIRP*, vol. 70, pp. 284–289, Jan. 2018.

[10] T. Butler and D. Wisner, "Exoskeleton technology: Making workers safer and more productive," *Prof. Saf.*, vol. 61, no. 9, pp. 32–36, Sep. 2016.

[11] K. Huysamen, T. Bosch, M. de Looze, K. S. Stadler, E. Graf, and L. W. O'Sullivan, "Evaluation of a passive exoskeleton for static upper limb activities," *Appl. Ergonom.*, vol. 70, pp. 148–155, Jul. 2018.

[12] M. C. Doyle, "Adaptive ARM support systems and methods for use," U.S. Patent 20 140 158 839 A1, Jun. 12, 2013.

[13] H. Kazerooni, E. Hacker, L. Chen, W. Tung, N. Poon, and T. Yangyuenthanasan, "Trunk supporting exoskeleton and method of use," WO Patent 2 017 086 946 A1, Dec. 21, 2017.

[14] D. J. Hyun, K. Bae, K. Kim, S. Nam, and D.-H. Lee, "A light-weight passive upper arm assistive exoskeleton based on multi-linkage spring-energy dissipation mechanism for overhead tasks," *Robot. Auto. Syst.*, vol. 122, Dec. 2019, Art. no. 103309.

[15] T. Nef and R. Riener, "Shoulder actuation mechanisms for arm rehabilitation exoskeletons," in *Proc. 2nd IEEE RAS EMBS Int. Conf. Biomed. Robot. Biomechatronics*, Oct. 2008, pp. 862–868.

[16] Y. Jung and J. Bae, "Kinematic analysis of a 5-DOF upper-limb exoskeleton with a tilted and vertically translating shoulder joint," *IEEE/ASME Trans. Mechatronics*, vol. 20, no. 3, pp. 1428–1439, Jun. 2015.

[17] J. Yoon, S. Kim, J. Moon, J. Kim, and G. Lee, "Minimizing misalignment and frame protrusion of shoulder exoskeleton via optimization for reducing interaction force and minimizing volume," *Machines*, vol. 10, no. 12, p. 1223, Dec. 2022.

[18] J. Kim, J. Kim, Y. Jung, D. Lee, and J. Bae, "A passive upper limb exoskeleton with tilted and offset shoulder joints for assisting overhead tasks," *IEEE/ASME Trans. Mechatronics*, vol. 27, no. 6, pp. 4963–4973, Dec. 2022.

[19] D. Park, S. Toxiri, G. Chini, C. D. Natali, D. G. Caldwell, and J. Ortiz, "Shoulder-sideWINDER (shoulder-side wearable INDustrial ergonomic robot): Design and evaluation of shoulder wearable robot with mechanisms to compensate for joint misalignment," *IEEE Trans. Robot.*, vol. 38, no. 3, pp. 1460–1471, Jun. 2022.

[20] M. Rossini et al., "Design and evaluation of a passive cable-driven occupational shoulder exoskeleton," *IEEE Trans. Med. Robot. Bionics*, vol. 3, no. 4, pp. 1020–1031, Nov. 2021.

[21] F. Balser, R. Desai, A. Ekizoglou, and S. Bai, "A novel passive shoulder exoskeleton designed with variable stiffness mechanism," *IEEE Robot. Autom. Lett.*, vol. 7, no. 2, pp. 2748–2754, Apr. 2022.

[22] L. Grazi, E. Trigili, G. Proface, F. Giovacchini, S. Crea, and N. Vitiello, "Design and experimental evaluation of a semi-passive upper-limb exoskeleton for workers with motorized tuning of assistance," *IEEE Trans. Neural Syst. Rehabil. Eng.*, vol. 28, no. 10, pp. 2276–2285, Oct. 2020.

[23] A. Zahedi, Y. Wang, N. Lau, W. T. Ang, and D. Zhang, "A bamboo-inspired exoskeleton (BiEXO) based on carbon fiber for shoulder and elbow joints," *IEEE Trans. Med. Robot. Bionics*, vol. 5, no. 2, pp. 375–386, May 2023.

[24] P. Maurice et al., "Objective and subjective effects of a passive exoskeleton on overhead work," *IEEE Trans. Neural Syst. Rehabil. Eng.*, vol. 28, no. 1, pp. 152–164, Jan. 2020.

[25] B. van Ninhuijs, J. W. Jansen, B. L. J. Gysen, and E. A. Lomonova, "Multi-degree-of-freedom spherical permanent-magnet gravity compensator for mobile arm support systems," *IEEE Trans. Ind. Appl.*, vol. 50, no. 6, pp. 3628–3636, Nov. 2014.

[26] J. Boisclair, P.-L. Richard, T. Laliberté, and C. Gosselin, "Gravity compensation of robotic manipulators using cylindrical Halbach arrays," *IEEE/ASME Trans. Mechatronics*, vol. 22, no. 1, pp. 457–464, Feb. 2017.

[27] K.-W. Jeon, H.-J. Chung, E.-J. Jung, J.-S. Kang, S.-E. Son, and H. Yi, "Development of shoulder muscle-assistive wearable device for work in unstructured postures," *Machines*, vol. 11, no. 2, p. 258, Feb. 2023.

[28] K.-X. Qian, P. Zeng, W.-M. Ru, and H.-Y. Yuan, "Novel magnetic spring and magnetic bearing," *IEEE Trans. Magn.*, vol. 39, no. 1, pp. 559–561, Jan. 2003.

[29] S.-W. Seo, Y.-H. Kim, J.-H. Lee, and J.-Y. Choi, "Analytical torque calculation and experimental verification of synchronous permanent magnet couplings with Halbach arrays," *AIP Adv.*, vol. 8, no. 5, Dec. 2017, Art. no. 056609.

[30] K. Li, J. Z. Bird, and V. M. Acharya, "Ideal radial permanent magnet coupling torque density analysis," *IEEE Trans. Magn.*, vol. 53, no. 6, pp. 1–4, Jun. 2017.

[31] W. T. Dempster and G. R. L. Gaughran, "Properties of body segments based on size and weight," *Amer. J. Anatomy*, vol. 120, no. 1, pp. 33–54, Jan. 1967.

[32] V. Zumstein, M. Kraljević, S. Hoechel, A. Conzen, A. Nowakowski, and M. Müller-Gerbl, "The glenohumeral joint—A mismatching system? A morphological analysis of the cartilaginous and osseous curvature of the humeral head and the glenoid cavity," *J. Orthopaedic Surg. Res.*, vol. 9, no. 1, p. 34, 2014.

[33] T. Nakayama et al., "Appropriate needle lengths determined using ultrasonic echograms for intramuscular injections in Japanese infants," *Open J. Pediatrics*, vol. 6, no. 2, pp. 163–170, 2016.

[34] C. Liu, H. Liang, N. Ueda, P. Li, Y. Fujimoto, and C. Zhu, "Functional evaluation of a force sensor-controlled upper-limb power-assisted exoskeleton with high backdrivability," *Sensors*, vol. 20, no. 21, p. 6379, Nov. 2020.

[35] (Sep. 2023). *SENIAM*. [Online]. Available: https://www.seniam.org/

[36] M. J. Diener, "Cohen's D," in *The Corsini Encyclopedia of Psychology*, 2010. [Online]. Available: https://doi.org/10.1002/9780470479216.corpsy0200

[37] M. Asgari, P. T. Hall, B. S. Moore, and D. L. Crouch, "Wearable shoulder exoskeleton with spring-cam mechanism for customizable, nonlinear gravity compensation," in *Proc. 42nd Annu. Int. Conf. IEEE Eng. Med. Biol. Soc. (EMBC)*, Jul. 2020, pp. 4926–4929.

[38] S. De Bock et al., "An occupational shoulder exoskeleton reduces muscle activity and fatigue during overhead work," *IEEE Trans. Biomed. Eng.*, vol. 69, no. 10, pp. 3008–3020, Oct. 2022.